frontiers in Chemistry

ORIGINAL RESEARCH
published: 31 May 2021
doi: 10.3389/fchem.2021.690833

NIR-II Upconversion Photoluminescence of Er^{3+} Doped $LiYF_4$ and $NaY(Gd)F_4$ Core-Shell Nanoparticles

*Qilong Feng†, Wenjing Zheng†, Jie Pu, Qiaoli Chen and Wei Shao**

College of Chemical Engineering and State Key Laboratory Breeding Base of Green Chemistry Synthesis Technology, Zhejiang University of Technology, Hangzhou, China

The availability of colloidal nano-materials with high efficiency, stability, and non-toxicity in the near infrared-II range is beneficial for biological diagnosis and therapy. Rare earth doped nanoparticles are ideal luminescent agents for bio-applications in the near infrared-II range due to the abundant energy level distribution. Among them, both excitation and emission range of Er^{3+} ions can be tuned into second biological window range. Herein, we report the synthesis of ~15 nm $LiYF_4$, $NaYF_4$, and $NaGdF_4$ nanoparticles doped with Er^{3+} ions and their core-shell structures. The luminescent properties are compared, showing that Er^{3+} ions with single-doped $LiYF_4$ and $NaYF_4$ nanoparticles generate stronger luminescence than Er^{3+} ions with doped $NaGdF_4$, despite the difference in relative intensity at different regions. By epitaxial growth an inert homogeneous protective layer, the surface luminescence of the core-shell structure is further enhanced by about 5.1 times, 6.5 times, and 167.7 times for $LiYF_4$, $NaYF_4$, and $NaGdF_4$, respectively. The excellent luminescence in both visible and NIR range of these core-shell nanoparticles makes them potential candidate for bio-applications.

Keywords: upconversion, NIR-II, core-shell, Er^{3+}, luminescence

OPEN ACCESS

Edited by:
Jiawei Zhang,
Clemson University, United States

Reviewed by:
Zhongzheng Yu,
Nanyang Technological University, Singapore
Ruichan Lv,
Xidian University, China

****Correspondence:***
Wei Shao
weishao@zjut.edu.cn

†These authors have contributed equally to this work

Specialty section:
This article was submitted to Nanoscience, a section of the journal Frontiers in Chemistry

Received: *08 April 2021*
Accepted: *26 April 2021*
Published: *31 May 2021*

Citation:
Feng Q, Zheng W, Pu J, Chen Q and Shao W (2021) NIR-II Upconversion Photoluminescence of Er^{3+} Doped $LiYF_4$ and $NaY(Gd)F_4$ Core-Shell Nanoparticles. Front. Chem. 9:690833. doi: 10.3389/fchem.2021.690833

INTRODUCTION

The 4f-4f transition of rare earth elements endows them with outstanding optical properties. Specifically, the energy of photons can be converted through rational designed transition among their abundant energy levels (Auzel, 2004; Wen et al., 2018). Furthermore, the photo-luminescence of rare earth is extremely stable, and it could not be affected by blinking or photobleaching (Shao et al., 2018; Song et al., 2019). These advantages make rare earth elements perfect candidates for light-triggered diagnostics and therapy (Chen et al., 2014; Shao et al., 2016; Qiang and Wang, 2019; Wang et al., 2020). As an unusual anti-stokes process, photon upconversion (UC) refers to converting several low-energy photons to one high-energy photon (Zhou et al., 2015; Wei et al., 2016). Due to the non-linear instincts, UC materials are well-developed for bio-imaging (Gonzalez-Bejar et al., 2016; Chen et al., 2021), photo-dynamics therapy(Lucky et al., 2015; Liu et al., 2019; Jia et al., 2020), and single particle imaging (Gargas et al., 2014; Liu et al., 2017; Zhou et al., 2020b; Dong et al., 2021).

The penetration depth of photons with different energies is significantly varied due to the scattering and absorption of biological tissue (Hemmer et al., 2016; Li and Wang, 2018). Compared to the visible range, where the auto-fluorescence of most tissue components is located, the near-infrared (NIR) range generally exhibits better spatial resolution and sharper contrast (Kenry et al.,

2018). Recent studies have demonstrated that probes utilized in biological window II (1000–1700 nm, NIR-II) work more effectively than that in biological window I (700–900 nm, NIR-I) (He et al., 2015; Zhong et al., 2017; Fan et al., 2018; Huang et al., 2020; Lin et al., 2021; Lv et al., 2021; Yu et al., 2021). However, most reports on NIR probes are realized in the first biological window (Zhou et al., 2020a). Meanwhile, upconversion and down-shifting of rare earth with emission in biological window II have gained considerable interest recently. Zhong et al. have designed an Er-based nanoparticle (NPs) doped with Ce^{3+}, which enhanced the down-shifting emission at 1550 nm under excitation at 980 nm (Zhong et al., 2017). They acquired high spatiotemporal resolution cerebral vasculatures in the NIR-II window with short exposure time. Liu et al. synthesized Er and Ho co-doped NPs with both excitation and emission in the NIR-II window as a sensor for inflammation dynamic detection (Liu et al., 2018). The time-gate imaging technique in the NIR-II window was realized in a $NaYF_4$: Yb, Nd@CaF_2 core shell structure with outstanding brightness (Tan et al., 2020). Er^{3+} ion is known as an outstanding imaging agent for NIR-II range, since it can be excited around 1550 nm due to the $^4I_{15/2} \rightarrow {}^4I_{13/2}$ transition (Chen et al., 2011; Shao et al., 2014; Cheng et al., 2018). Moreover, the emission peaks are at 550 nm ($^4S_{3/2} \rightarrow {}^4I_{15/2}$) and 660 nm ($^4F_{9/2} \rightarrow {}^4I_{15/2}$) in the visible range, 800 nm ($^4I_{9/2} \rightarrow {}^4I_{15/2}$) in the NIR-I range, and 1000 nm ($^4I_{11/2} \rightarrow {}^4I_{15/2}$) in the NIR-II range, respectively. The two-photon NIR-II to NIR-II UC process is rather unique, which have been investigated widely. However, how the matrix determines the luminescence remains unknown and deserves our efforts.

Herein, we reported the successful synthesis of three types of fluoride matrix, $LiYF_4$, $NaYF_4$, and $NaGdF_4$, each one doped with Er^{3+} ions. Their luminescence properties were compared, showing different relative intensity within each matrix. With epitaxial growth an inert homogeneous protect layer, the luminescence of each kind of UCNPs achieve much improvement due to the surface passivation. A proper mechanism was proposed based on the emission intensity dependence on excitation power density.

MATERIALS AND METHODS

Materials

Yttrium (III) chloride hexahydrate (99.99%), erbium (III) chloride hexahydrate (99.9%), gadolinium (III) chloride hexahydrate (99.9%), yttrium (III) oxide (99.999%), gadolinium (III) oxide (99.9%), sodium trifluoroacetate (98%), lithium trifluoroacetate (95%), trifluoroacetic acid (98%), 1-octadecene (90%), and oleic acid (90%) were purchased from Sigma-Aldrich. Sodium hydroxide (98%), lithium hydroxide (98%), and ammonium fluoride (98%) were purchased from Aladdin Co. All chemicals were used as received.

Instruments

The size and morphology of the resulting nanoparticles were characterized by Hitachi 7700 electron microscope. Upconversion emission spectra in visible and NIR range were recorded using Horiba Fluoromax–4. Laser excitation at 1532 nm, which was purchased from Changchun New Industries Optoelectronics Technology Co., Ltd. The emission signal from the sample in the cuvette was collected at 90° relative to the exciting laser beam. The powder X-ray diffraction (XRD) patterns were recorded by a Bruker D8 Advance diffractometer using Cu Kα radiation. The 2θ angle of the XRD spectra was recorded at a scanning rate of 5°/min.

Synthesis of $LiYF_4$:10%Er^{3+} ($NaYF_4$:10%Er^{3+} and $NaGdF_4$:10%Er^{3+})

In a typical procedure, a total of 0.1°mmol $ErCl_3 \bullet H_2O$ and 0.9°mmol $YCl_3 \bullet H_2O$ were added into a 100°ml flask containing 6°ml oleic acid and 15°ml octadecene. The mixture was heated to 160°C for 60°min then cooled down to room temperature. Subsequently, a solution of 4°mmol NH_4F and 2.5°mmol LiOH (2.5°mmol NaOH for $NaYF_4$:10%Er^{3+} and $NaGdF_4$:10%Er^{3+}) in 10°ml methanol was added and stirred for 30°min. The reaction mixture was then heated at 100°C for 30°min to remove the methanol, followed by heating up to 290°C (300°C for $NaYF_4$: 10%Er^{3+} and $NaGdF_4$:10%Er^{3+}) and keeping for 60°min before cooling down. A syringe needle was used to let the argon gas out during the synthesis. The mixture was cooled to room temperature and precipitated by excess ethanol and collected by centrifugation. The precipitate was washed with ethanol several times, and the nanocrystals were finally dispersed in hexane.

Synthesis of $LiYF_4$:10%Er^{3+}@$LiYF_4$ ($NaYF_4$: 10%Er^{3+}@$NaYF_4$, $NaGdF_4$:10%Er^{3+}@ $NaGdF_4$)

The $LiYF_4$:10%Er^{3+}@$LiYF_4$ core-shell nanoparticles are synthesized via a thermal decomposition method. A total of 0.5°mmol of Y_2O_3 was dissolved in 50% trifluoroacetic acid at 95°C in a three-neck flask. Then, the solutions were evaporated to dryness under an argon gas purge. Next, 10°ml of oleic acid, 10°ml of 1-octadecene, 1.5°mmol lithium trifluoroacetate, and 1°mmol $LiYF_4$:10%Er^{3+} core (2°mmol sodium trifluoroacetate and 1°mmol $NaYF_4$:10%Er^{3+} core for $NaYF_4$:10%Er^{3+}@$NaYF_4$, 2°mmol sodium trifluoroacetate and 1°mmol $NaGdF_4$:10%Er^{3+} core for $NaGdF_4$: 10%Er^{3+}@$NaGdF_4$) were added into the flask. The resulting solution was then heated at 120°C with magnetic stirring for 45°min to remove water and oxygen. The brown solution was then heated to 310°C at a rate of about 12°C per min under argon gas protection and kept at this temperature under vigorous stirring for 45°min. A syringe needle was used to let the argon gas out during the synthesis. The mixture was cooled to room temperature and precipitated by excess ethanol and collected by centrifugation. The precipitate was washed with ethanol several times, and the nanocrystals were dispersed in hexane.

RESULTS AND DISCUSSION

In order to evaluate the emission intensity impacted by matrix, 10% Er^{3+} was doped into three matrix $LiYF_4$, $NaYF_4$ and $NaGdF_4$ according to a previous synthesis procedure (Wang et al., 2010b).

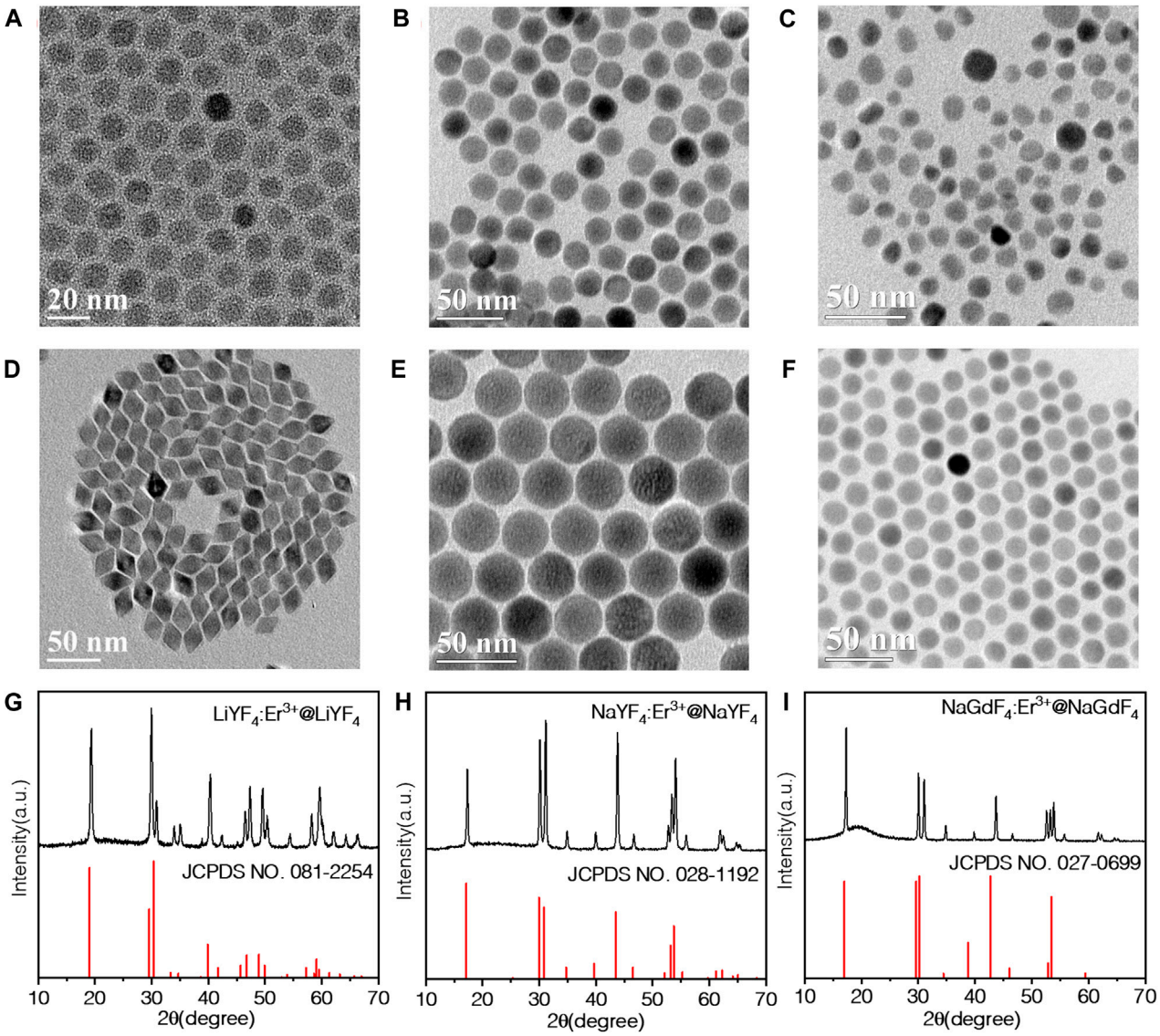

FIGURE 1 | TEM images of **(A)** $LiYF_4$:10%Er^{3+}, **(B)** $NaYF_4$:10%Er^{3+}, **(C)** $NaGdF_4$:10%Er^{3+}, **(D)** $LiYF_4$:10%Er^{3+}@$LiYF_4$, **(E)** $NaYF_4$:10%Er^{3+}@$NaYF_4$, **(F)** $NaGdF_4$:10%Er^{3+}@$NaGdF_4$ nanoparticles; and XRD pattern of **(G)** $LiYF_4$:10%Er^{3+}@$LiYF_4$, **(H)** $NaYF_4$:10%Er^{3+}@$NaYF_4$, **(I)** $NaGdF_4$:10%Er^{3+}@$NaGdF_4$ nanoparticles.

These three matrix types have been investigated extensively due to their low phonon energy (~400˚cm^{-1}), which are beneficial for efficient UC luminescence. As shown in **Figure 1**, three types of UCNPs were all monodisperse in hexanes solvents. $LiYF_4$ was shaped with spindle morphology (**Figure 1A**), while $NaYF_4$ (**Figure 1B**) and $NaGdF_4$ (**Figure 1C**) were shaped with the spheric shape, respectively. The size of $LiYF_4$ is determined to be around 16 nm, $NaYF_4$ around 19 nm, and $NaGdF_4$ 14 nm (**Supplementary Figures S1A–C**), which makes them comparable since the luminescences of NPs are significantly effected by their sizes. The X-ray diffraction (XRD) pattern in **Supplementary Figure S2** showed the $LiYF_4$ possessed tetragonal phase, which was accordance with previous report. However, a hexagonal phase was identified for $NaYF_4$, and a mixed hexagonal and cubic phase for $NaGdF_4$ as the peaks at ~27.5˚ and ~32.5˚ referred to the (111) and (200) plane of the cubic phase of $NaGdF_4$. Previous reports have concluded doping ions with larger size will efficiently reduce the energy and time for transformation from cubic to hexagonal phase (Wang et al., 2010a). Considering the reverse, a smaller size dopant is supposed to increase the energy barrier of transformation and reduce the stability of the hexagonal phase. In our case, the dopant size of Er^{3+} ion is 1.144 Å, which is smaller than Gd^{3+} (1.193 Å) and Y^{3+} (1.159 Å). The differential between Gd^{3+} and Er^{3+} is more remarkable than that of Y^{3+} and Er^{3+}. As a result, the $NaGdF_4$ requires more energy to complete the phase transfer. Then we further grew a homogeneous shell on each type of core UCNP as protect layer since the inert epitaxial shell growth could enhance the UC luminescence by overcoming the concentration quenching effects. The Transmission electron microscopy

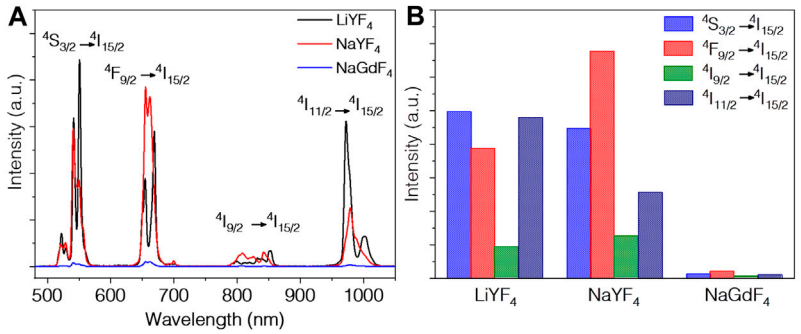

FIGURE 2 | (A) UC emission spectra and **(B)** integration of all peaks of $LiYF_4$:10%Er^{3+}, $NaYF_4$:10%Er^{3+}, $NaGdF_4$:10%Er^{3+} nanoparticles excited at 1532 nm.

(TEM) imaging shows the sizes of three types of NPs grow larger, and the morphologies are much more uniform and monodisperse after coating the shell layer (**Figure 1D–F**). The size increase in the core-shell NPs is shown in **Supplementary Figures S1D–F**, and this proved the successful coating of shell on the core NPS. The phase of these core-shell UCNPs remain the same with core NPs, except $NaGdF_4$ change from the fixed cubic and hexagonal phase to pure hexagonal phase (**Supplementary Figures S1G–I**). We believe the shell coating process provides enough energy for the phase transfer of $NaGdF_4$ as well as epitaxial growth.

The UC properties of three core NPs under 1532 nm excitation were compared. As shown in **Figure 2**, three types of core NPs all emit four characteristic peaks assigned to the $^4S_{3/2} \rightarrow {}^4I_{15/2}$ (550 nm), $^4F_{9/2} \rightarrow {}^4I_{15/2}$ (660 nm), $^4I_{9/2} \rightarrow {}^4I_{15/2}$ (800 nm), and $^4I_{11/2} \rightarrow {}^4I_{15/2}$ (1000 nm), respectively. The optimized concentration of Er^{3+} ions is determined to be 10% according to integration of the total emission intensity (**Supplementary Figure S3**). The emission intensity of $NaYF_4$ core UCNPs is almost the same with $LiYF_4$, which is about 50 times stronger than $NaGdF_4$ UCNPs (**Supplementary Figure S4**). We further integrated the emission intensities of each peak for all three core NPs, respectively, as illustrated in **Figure 2B**. Notably, the $^4F_{9/2} \rightarrow {}^4I_{15/2}$ transition (660 nm) of $NaYF_4$ is about 1.7 times stronger than $LiYF_4$, while on the contrary, the $^4I_{11/2} \rightarrow {}^4I_{15/2}$ transition (1000 nm) of $LiYF_4$ is about twice of the $NaYF_4$. As we all know, the luminescence of rare earth can be ascribed to the local field splitting, which is highly depended on the crystal symmetry. Then it is understandable the tetragonal and hexagonal phases with different symmetry structures will favor variable energy transition, corresponding to the diverse dominant luminescence character. This explains the intensities of different peaks are not identical for the $NaYF_4$ and $LiYF_4$ matrix, and so the NIR-II emission bands of $LiYF_4$:Er^{3+} are more suitable than $NaYF_4$:Er^{3+} NPs. As for the $NaGdF_4$, it contains both cubic and hexagonal phase. For the parity forbidden essence, the phase with lower symmetry exhibits stronger emission intensity than the phase with higher symmetry (Liu, 2015). The luminescence of hexagonal phase $NaGdF_4$ is always much stronger than the cubic phase, so the mixed phase $NaGdF_4$ emits less efficient than pure hexagonal phase $NaYF_4$ (Damasco et al., 2014).

For rare earth nanomaterials, the protection shell architecture can suppress the surface-related quenching effects. Especially for Er^{3+} heavily doped nanoparticles, the core-shell architecture can significantly enhance both the UC and down-shifting luminescence. The concentration quenching of bare core is contributed mainly by surface quenching of defects and high phonon ligand instead of common misconceptions of cross-relaxation of rare earth (Johnson et al., 2017). Indeed, by coating a homogeneous shell, the luminescent intensity is unanimously enhanced for all the UCNPs, specifically, 5.1 times for $LiYF_4$, 6.5 times for $NaYF_4$, and 167.7 times for $NaGdF_4$, as shown in **Figure 3**. The enhancement of $LiYF_4$ nanoparticles and $NaYF_4$ nanoparticles is similar, which illustrates surface passivation is the dominant factor rather than the crystal phase, since the sizes of core $LiYF_4$ and $NaYF_4$ UCNPs are almost the same. Compared to $LiYF_4$ and $NaYF_4$, the increase in the luminescence of $NaGdF_4$ is more remarkable. As mentioned above, the shell growth on $NaGdF_4$ includes two processes: complete phase transfer from the mixed phase to pure hexagonal phase together with the epitaxial growth of protection shell. Two processes all result in considerable emission enhancement to the extent that the total luminescence of $NaGdF_4$:Er^{3+}@$NaGdF_4$ is as high as that of $LiYF_4$:Er^{3+}@$LiYF_4$ core-shell UCNPs. The luminescence of $NaYF_4$:Er^{3+}@$NaYF_4$ is slightly higher than the other two types of UCNPs by about 1.6 times. Moreover, the emission intensity around 1000 nm of $LiYF_4$:Er^{3+}@$LiYF_4$ core-shell UCNPs is slightly higher than $NaYF_4$:Er^{3+}@$NaYF_4$ UCNPs. All three types of core-shell UCNPs exhibit excellent emission in visible and NIR range, showing great potential for NIR-II range bio-applications.

Then, we measured the pump power dependences of four bands for the colloidal $LiYF_4$:Er^{3+}@$LiYF_4$ core-shell UCNPs. As shown in **Figure 4A**, all the bands show a slope around 1, which is deviated from the reported UC mechanism. It is well established when the UC rate exceeds the decay rate for the intermediated states, the dependence on the excitation power P will decrease from P^n to P^1. In our case, the saturation of $^4I_{13/2}$ energy levels will cause such phenomenons, which explains the smaller measured photon numbers. These data are well accordance with previous literature, revealing similar energy transfer UC mechanism (Chen et al., 2011; Shao et al., 2014). Briefly, directly excitation of Er^{3+} ions by 1532 nm laser promotes the transition from $^4I_{15/2}$ to $^4I_{13/2}$.

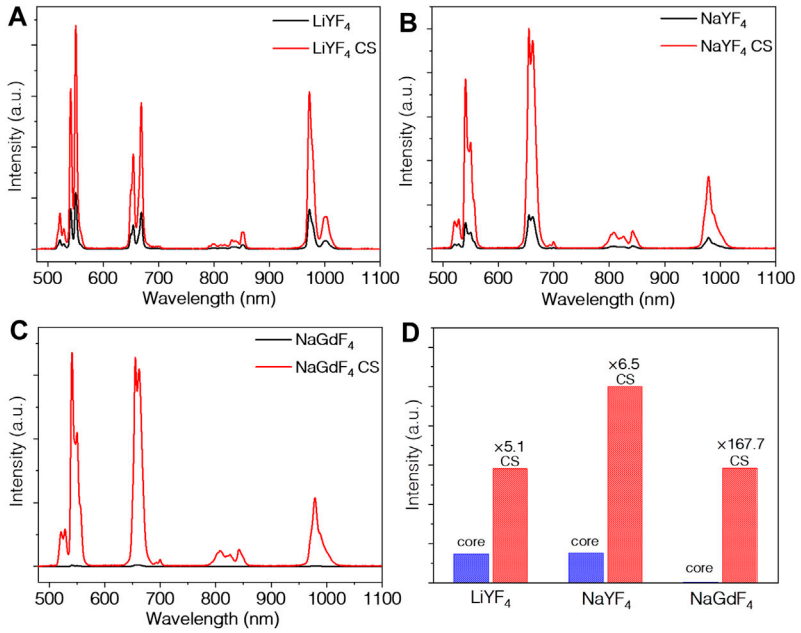

FIGURE 3 | UC emission spectra of **(A)** $LiYF_4$:10%Er^{3+} and $LiYF_4$:10%Er^{3+}@$LiYF_4$, **(B)** $NaYF_4$:10%Er^{3+} and $NaYF_4$:10%Er^{3+}@$NaYF_4$, **(C)** $NaGdF_4$:10%Er^{3+} and $NaGdF_4$:10%Er^{3+}@$NaGdF_4$ nanoparticles, and **(D)** the integration of their emission peaks excited at 1532 nm.

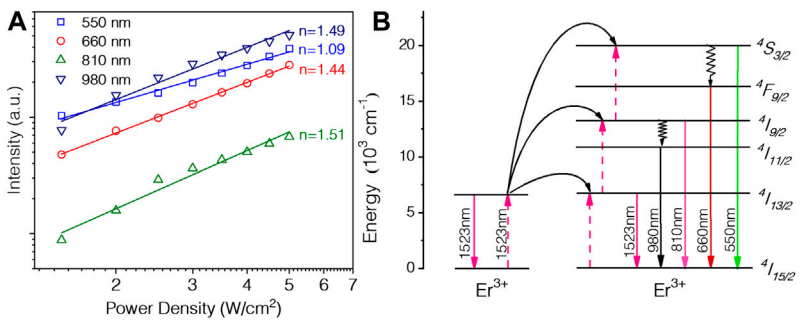

FIGURE 4 | (A) Dependence of four peaks versus pump power, and **(B)** the proposed energy transfer upconversion mechanism between Er^{3+} ions.

Then three-photon energy transfer process generates both green ($^4S_{3/2}$) and red ($^4F_{9/2}$) emission bands as well as the two-photon process of 800 nm ($^4I_{9/2}$) and 980 nm ($^4I_{11/2}$) emission peaks.

CONCLUSION

In conclusion, we have observed four intensive emission bands for three colloidal and uniform $LiYF_4$:Er^{3+}@$LiYF_4$, $NaYF_4$:Er^{3+}@$NaYF_4$, and $NaGdF_4$:Er^{3+}@$NaGdF_4$ core-shell UCNPs under excitation at 1532 nm. Homogeneous epitaxial growth of the shell layer promoted the luminescence intensity efficiently. Notably, $NaGdF_4$ completed the phase transfer during the shell coating, which enhanced the core luminescence intensity about 167.7 folds. Taking $LiYF_4$:Er^{3+}@$LiYF_4$ as example, the intensities of four UC peaks showed linear dependence on the excitation power, which can be explained by a saturation effect of $^4I_{13/2}$ energy level. These core-shell UCNPs are pronounced as ideal NIR-II agent for biological related applications.

DATA AVAILABILITY STATEMENT

The original contributions presented in the study are included in the article/**Supplementary Material**, further inquiries can be directed to the corresponding author.

AUTHOR CONTRIBUTIONS

QF, WZ, JP conducted the synthesis and optical measurement under supervision of WS and QC.

FUNDING

This work is supported by the National Natural Science Foundation of China (51802281), and the Zhejiang Provincial Natural Science Foundation (LY21B010006).

SUPPLEMENTARY MATERIAL

The Supplementary Material for this article can be found online at: https://www.frontiersin.org/articles/10.3389/fchem.2021.690833/full#supplementary-material

REFERENCES

Auzel, F. (2004). Upconversion and Anti-stokes Processes with F and D Ions in Solids. *Chem. Rev.* 104, 139–174. doi:10.1021/cr020357g

Chen, B., Wang, Y., Guo, Y., Shi, P., and Wang, F. (2021). NaYbF4@NaYF4 Nanoparticles: Controlled Shell Growth and Shape-dependent Cellular Uptake. *ACS Appl. Mater. Inter.* 13, 2327–2335. doi:10.1021/acsami.0c20757

Chen, G., Ohulchanskyy, T. Y., Kachynski, A., Ågren, H., and Prasad, P. N. (2011). Intense Visible and Near-Infrared Upconversion Photoluminescence in Colloidal LiYF4: Er3+ Nanocrystals under Excitation at 1490 Nm. *ACS Nano* 5, 4981–4986. doi:10.1021/nn201083j

Chen, G., Qiu, H., Prasad, P. N., and Chen, X. (2014). Upconversion Nanoparticles: Design, Nanochemistry, and Applications in Theranostics. *Chem. Rev.* 114, 5161–5214. doi:10.1021/cr400425h

Cheng, X. W., Pan, Y., Yuan, Z., Wang, X. W., Su, W. H., Yin, L. S., et al. (2018). Er3+ Sensitized Photon Upconversion Nanocrystals. *Adv. Funct. Mater.* 28, 1800208. doi:10.1002/adfm.201800208

Damasco, J. A., Chen, G., Shao, W., Ågren, H., Huang, H., Song, W., et al. (2014). Size-Tunable and Monodisperse Tm3+/Gd3+-Doped Hexagonal NaYbF4 Nanoparticles with Engineered Efficient Near Infrared-To-Near Infrared Upconversion for In Vivo Imaging. *ACS Appl. Mater. Inter.* 6, 13884–13893. doi:10.1021/am503288d

Dong, H., Sun, L. D., and Yan, C. H. (2021). Lanthanide-Doped Upconversion Nanoparticles for Super-resolution Microscopy. *Front. Chem.* 8. doi:10.3389/fchem.2020.619377

Fan, Y., Wang, P., Lu, Y., Wang, R., Zhou, L., Zheng, X., et al. (2018). Lifetime-engineered NIR-II Nanoparticles Unlock Multiplexed In Vivo Imaging. *Nat. Nanotech* 13, 941-946. doi:10.1038/s41565-018-0221-0

Gargas, D. J., Chan, E. M., Ostrowski, A. D., Aloni, S., Altoe, M. V. P., Barnard, E. S., et al. (2014). Engineering Bright Sub-10-nm Upconverting Nanocrystals for Single-Molecule Imaging. *Nat. Nanotech* 9, 300–305. doi:10.1038/nnano.2014.29

Gonzalez-Bejar, M., Frances-Soriano, L., and Perez-Prieto, J. (2016). Upconversion Nanoparticles for Bioimaging and Regenerative Medicine. *Front. Bioeng. Biotechnol.* 4, 47. doi:10.3389/fbioe.2016.00047

He, F., Yang, G., Yang, P., Yu, Y., Lv, R., Li, C., et al. (2015). A New Single 808 Nm NIR Light-Induced Imaging-Guided Multifunctional Cancer Therapy Platform. *Adv. Funct. Mater.* 25, 3966–3976. doi:10.1002/adfm.201500464

Hemmer, E., Benayas, A., Légaré, F., and Vetrone, F. (2016). Exploiting the Biological Windows: Current Perspectives on Fluorescent Bioprobes Emitting above 1000 Nm. *Nanoscale Horiz.* 1, 168–184. doi:10.1039/c5nh00073d

Huang, J., Li, J., Zhang, X., Zhang, W., Yu, Z., Ling, B., et al. (2020). Artificial Atomic Vacancies Tailor Near-Infrared II Excited Multiplexing Upconversion in Core-Shell Lanthanide Nanoparticles. *Nano Lett.* 20, 5236–5242. doi:10.1021/acs.nanolett.0c01539

Jia, T., Wang, Z., Sun, Q. Q., Dong, S. M., Xu, J. T., Zhang, F. M., et al. (2020). Intelligent Fe-Mn Layered Double Hydroxides Nanosheets Anchored with Upconversion Nanoparticles for Oxygen-Elevated Synergetic Therapy and Bioimaging. *Small* 16. doi:10.1002/smll.202001343

Johnson, N. J. J., He, S., Diao, S., Chan, E. M., Dai, H., and Almutairi, A. (2017). Direct Evidence for Coupled Surface and Concentration Quenching Dynamics in Lanthanide-Doped Nanocrystals. *J. Am. Chem. Soc.* 139, 3275–3282. doi:10.1021/jacs.7b00223

Kenry Duan, Y., and Liu, B. (2018). Recent Advances of Optical Imaging in the Second Near-Infrared Window. *Adv. Mater.* 30. doi:10.1002/adma.201802394

Li, C., and Wang, Q. (2018). Challenges and Opportunities for Intravital Near-Infrared Fluorescence Imaging Technology in the Second Transparency Window. *ACS Nano* 12, 9654–9659. doi:10.1021/acsnano.8b07536

Lin, B., Wu, J., Wang, Y., Sun, S., Yuan, Y., Tao, X., et al. (2021). Peptide Functionalized Upconversion/NIR II Luminescent Nanoparticles for Targeted Imaging and Therapy of Oral Squamous Cell Carcinoma. *Biomater. Sci.* 9, 1000–1007. doi:10.1039/d0bm01737j

Liu, G. (2015). Advances in the Theoretical Understanding of Photon Upconversion in Rare-Earth Activated Nanophosphors. *Chem. Soc. Rev.* 44, 1635–1652. doi:10.1039/c4cs00187g

Liu, J., Yang, F., Feng, M., Wang, Y., Peng, X., and Lv, R. (2019). Surface Plasmonic Enhanced Imaging-Guided Photothermal/Photodynamic Therapy Based on Lanthanide-Metal Nanocomposites under Single 808 Nm Laser. *ACS Biomater. Sci. Eng.* 5, 5051–5059. doi:10.1021/acsbiomaterials.9b01112

Liu, L., Wang, S., Zhao, B., Pei, P., Fan, Y., Li, X., et al. (2018). Er3+ Sensitized 1530 Nm to 1180 Nm Second Near-Infrared Window Upconversion Nanocrystals for In Vivo Biosensing. *Angew. Chem. Int. Ed.* 57, 7518–7522. doi:10.1002/anie.201802889

Liu, Y., Lu, Y., Yang, X., Zheng, X., Wen, S., Wang, F., et al. (2017). Amplified Stimulated Emission in Upconversion Nanoparticles for Super-resolution Nanoscopy. *Nature* 543, 229, 233. doi:10.1038/nature21366

Lucky, S. S., Soo, K. C., and Zhang, Y. (2015). Nanoparticles in Photodynamic Therapy. *Chem. Rev.* 115, 1990–2042. doi:10.1021/cr5004198

Lv, R., Wang, Y., Lin, B., Peng, X., Liu, J., Lü, W.-d., et al. (2021). Targeted Luminescent Probes for Precise Upconversion/NIR II Luminescence Diagnosis of Lung Adenocarcinoma. *Anal. Chem.* 93, 4984–4992. doi:10.1021/acs.analchem.1c00374

Qiang, Q. P., and Wang, Y. H. (2019). Effect of Mn2+ on Upconversion Emission, Thermal Sensing and Optical Heater Behavior of Yb3+ - Er( )(3+)Codoped NaGdF4 Nanophosphors. *Front. Chem.* 7, 425. doi:10.3389/fchem.2019.00425

Shao, W., Chen, G., Damasco, J., Wang, X., Kachynski, A., Ohulchanskyy, T. Y., et al. (2014). Enhanced Upconversion Emission in Colloidal (NaYF_4: Er3+)/NaYF_4 Core/shell Nanoparticles Excited at 1523 Nm. *Opt. Lett.* 39, 1386–1389. doi:10.1364/ol.39.001386

Shao, W., Chen, G., Kuzmin, A., Kutscher, H. L., Pliss, A., Ohulchanskyy, T. Y., et al. (2016). Tunable Narrow Band Emissions from Dye-Sensitized Core/Shell/Shell Nanocrystals in the Second Near-Infrared Biological Window. *J. Am. Chem. Soc.* 138, 16192–16195. doi:10.1021/jacs.6b08973

Shao, W., Lim, C.-K., Li, Q., Swihart, M. T., and Prasad, P. N. (2018). Dramatic Enhancement of Quantum Cutting in Lanthanide-Doped Nanocrystals Photosensitized with an Aggregation-Induced Enhanced Emission Dye. *Nano Lett.* 18, 4922–4926. doi:10.1021/acs.nanolett.8b01724

Song, N., Zhou, B., Yan, L., Huang, J. S., and Zhang, Q. Y. (2019). Understanding the Role of Yb-3(+) in the Nd/Yb Coupled 808-Nm-Responsive Upconversion. *Front. Chem.* 6, 673. doi:10.3389/fchem.2018.00673

Tan, M. L., Li, F., Cao, N., Li, H., Wang, X., Zhang, C. Y., et al. (2020). Accurate In Vivo Nanothermometry through NIR-II Lanthanide Luminescence Lifetime. *Small* 16, e2004118. doi:10.1002/smll.202004118

Wang, F., Han, Y., Lim, C. S., Lu, Y., Wang, J., Xu, J., et al. (2010a). Simultaneous Phase and Size Control of Upconversion Nanocrystals through Lanthanide Doping. *Nature* 463, 1061–1065. doi:10.1038/nature08777

Wang, J., Wang, F., Xu, J., Wang, Y., Liu, Y., Chen, X., et al. (2010b). Lanthanide-doped LiYF4 Nanoparticles: Synthesis and Multicolor Upconversion Tuning. *Comptes Rendus Chim.* 13, 731–736. doi:10.1016/j.crci.2010.03.021

Wang, Z. D., Hu, T. T., Liang, R. Z., and Wei, M. (2020). Application of Zero-Dimensional Nanomaterials in Biosensing. *Front. Chem.* 8, 320. doi:10.3389/fchem.2020.00320

Wei, W., Chen, G., Baev, A., He, G. S., Shao, W., Damasco, J., et al. (2016). Alleviating Luminescence Concentration Quenching in Upconversion Nanoparticles through Organic Dye Sensitization. *J. Am. Chem. Soc.* 138, 15130–15133. doi:10.1021/jacs.6b09474

Wen, S. H., Zhou, J. J., Zheng, K. Z., Bednarkiewicz, A., Liu, X. G., and Jin, D. Y. (2018). Advances in Highly Doped Upconversion Nanoparticles. *Nat. Commun.* 9, 2415. doi:10.1038/s41467-018-04813-5

Yu, Z. Z., Chan, W. K., Zhang, Y., and Tan, T. T. Y. (2021). Near-infrared-II Activated Inorganic Photothermal Nanomedicines. *Biomaterials* 269, 120459. doi:10.1016/j.biomaterials.2020.120459

Zhong, Y. T., Ma, Z. R., Zhu, S. J., Yue, J. Y., Zhang, M. X., Antaris, A. L., et al. (2017). Boosting the Down-Shifting Luminescence of Rare-Earth Nanocrystals for Biological Imaging beyond 1500 Nm. *Nat. Commun.* 8. doi:10.1038/s41467-017-00917-6

Zhou, B., Yan, L., Huang, J., Liu, X., Tao, L., and Zhang, Q. (2020a). NIR II-Responsive Photon Upconversion through Energy Migration in an Ytterbium Sublattice. *Nat. Photon.* 14, 760-766. doi:10.1038/s41566-020-00714-6

Zhou, J., Li, C. Y., Li, D. H., Liu, X. F., Mu, Z., Gao, W. B., et al. (2020b). Single-molecule Photoreaction Quantitation through Intraparticle-Surface Energy Transfer (I-SET) Spectroscopy. *Nat. Commun.* 11. doi:10.1038/s41467-020-18223-z

Zhou, J., Liu, Q., Feng, W., Sun, Y., and Li, F. (2015). Upconversion Luminescent Materials: Advances and Applications. *Chem. Rev.* 115, 395–465. doi:10.1021/cr400478f

Conflict of Interest: The authors declare that the research was conducted in the absence of any commercial or financial relationships that could be construed as a potential conflict of interest.